ACS APPLIED MATERIALS & INTERFACES

Research Article

www.acsami.org

Chemical Sensing of 2D Graphene/MoS_2 Heterostructure device

Byungjin Cho,*[,†,∥] Jongwon Yoon,[‡,∥] Sung Kwan Lim,[‡] Ah Ra Kim,[†] Dong-Ho Kim,[†] Sung-Gyu Park,[†] Jung-Dae Kwon,[†] Young-Joo Lee,[†] Kyu-Hwan Lee,[§] Byoung Hun Lee,[‡] Heung Cho Ko,*[,‡] and Myung Gwan Hahm*[,†]

[†]Department of Advanced Functional Thin Films, Surface Technology Division, Korea Institute of Materials Science (KIMS), 797 Changwondaero, Sungsan-Gu, Changwon, Gyeongnam 642-831, Republic of Korea

[‡]School of Materials Science and Engineering, Gwangju Institute of Science and Technology (GIST), 261 Cheomdan-gwagiro, Buk-Gu, Gwangju 500-712, Republic of Korea

[§]Electrochemistry Department, Surface Technology Division, Korea Institute of Materials Science (KIMS), 797 Changwondaero, Sungsan-Gu, Changwon, Gyeongnam 642-831, Republic of Korea

Supporting Information

ABSTRACT: We report the production of a two-dimensional (2D) heterostructured gas sensor. The gas-sensing characteristics of exfoliated molybdenum disulfide (MoS_2) connected to interdigitated metal electrodes were investigated. The MoS_2 flake-based sensor detected a NO_2 concentration as low as 1.2 ppm and exhibited excellent gas-sensing stability. Instead of metal electrodes, patterned graphene was used for charge collection in the MoS_2-based sensing devices. An equation based on variable resistance terms was used to describe the sensing mechanism of the graphene/MoS_2 device. Furthermore, the gas response characteristics of the heterostructured device on a flexible substrate were retained without serious performance degradation, even under mechanical deformation. This novel sensing structure based on a 2D heterostructure promises to provide a simple route to an essential sensing platform for wearable electronics.

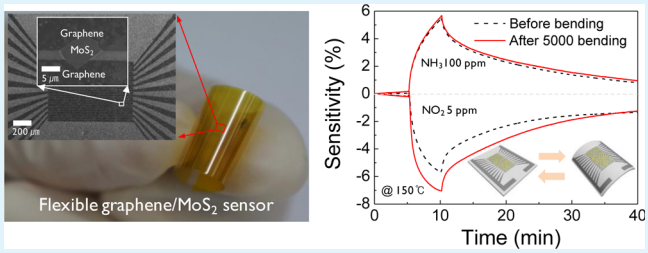

KEYWORDS: *MoS_2, graphene, gas sensor, heterostructure, flexible device*

INTRODUCTION

In recent years, atomically layered transition metal dichalcogenides (TMDs), which are distinct from van der Waals (vdW)-stacked bulk TMDs, have stimulated intensive research due to their intriguing physical properties and versatile electronic applications.[1−9] Molybdenum disulfide (MoS_2) has been a major focus of these studies.[10,11] The use of single atomic layers of MoS_2 offers extremely large surface-to-volume ratios, low power consumption, high compatibility for integration with conventional Si technology, and inherent flexibility. The successful demonstration of quasi-two-dimensional (2D) MoS_2-based field-effect transistors,[11−15] photodetectors,[16,17] and gas sensors[18−21] has motivated an exploration of the unusual physical properties of MoS_2 atomic layers.

The ultimate goal of the development of nanomaterial-based electronic devices is to produce atomically stacked 2D architectures via synergistic combinations of atomic-layered nanomaterials with dissimilar physical properties; such devices are often referred to as vdW heterostructure devices.[22−26] Strong covalent bonds in-plane and relatively weak vdW interactions out-of-plane provide the structural stability for these atomic-scale heterostructures.[22] Various types of such heterostructures have been investigated recently, enabling elucidation of the underlying physics.[23,24] A recent flurry of activity in this research field involves the interesting characteristics of a diverse range of low-dimensional heterostructures, such as h-BN−graphene,[27] TMD−TMD,[24,26] and TMD−graphene.[28] However, these low-dimensional heterostructures mostly have been limited to field-effect transistor and photonic applications.[3] Gas-phase detection involving TMDs, especially MoS_2, has exhibited an extraordinary sensing capability that is superior to that of carbon-based nanomaterials.[19] A structural advantage of MoS_2, such as its high surface-to-volume ratio, can be translated into highly sensitive gas-sensor applications via charge transfer on the surface of MoS_2.[29,30] Graphene can also be used to detect individual molecules, leading to the ultimate sensitivity.[31] Therefore, it is imperative to fabricate and investigate a novel 2D sensing platform utilizing 2D heterostructures. Furthermore, the flexible gas-sensing capability of such 2D heterostructures for wearable electronics should also be verified.

Here, we report the development of an atomically thin heterostructure-based gas sensor via a combination of mechanically exfoliated MoS_2 and graphene synthesized via

Received: May 25, 2015
Accepted: July 10, 2015
Published: July 10, 2015

DOI: 10.1021/acsami.5b04541
ACS Appl. Mater. Interfaces 2015, 7, 16775−16780

chemical vapor deposition (CVD). First, we explored the gas-sensing capability of the MoS_2-based device. The exfoliated MoS_2 connected to interdigitated metal electrodes functions as an active nanomaterial for detecting gas molecules. The detection limit of the MoS_2 flake-based gas sensor was 1.2 ppm of NO_2, and the sensor exhibited excellent gas-sensing stability. Second, a patterned graphene film, substituting for metal electrodes, was used for charge collection of the MoS_2-based sensing devices. On the basis of an equation of the variable resistance terms, the sensing mechanism of the graphene/MoS_2 device was examined in detail. Furthermore, the gas-response characteristics of the flexible graphene/MoS_2 device were well maintained, without any serious performance degradation, even after a harsh bending test. The 2D heterostructure provides a simple route to an essential sensing component of wearable electronics.

RESULTS AND DISCUSSION

Figure 1a shows an Au/Ti/MoS_2 device comprised of MoS_2 flakes exfoliated using the Scotch tape method and

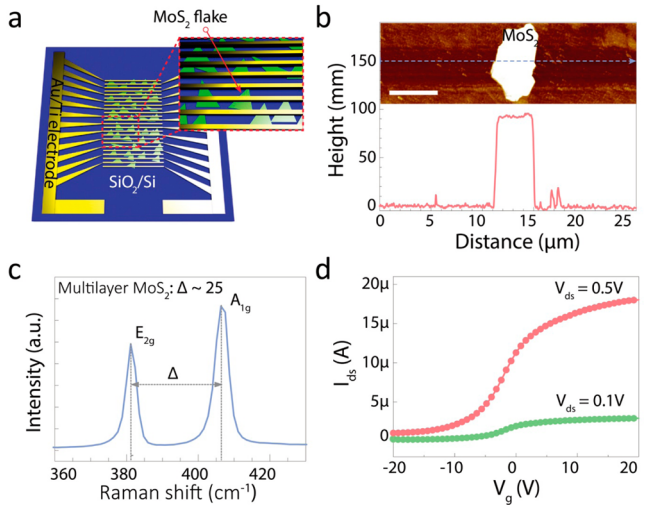

Figure 1. MoS_2 device with Au/Ti interdigitated electrodes. (a) Schematic image of MoS_2 flakes bridging Au/Ti interdigitated electrodes. (b) AFM height profile of a MoS_2 flake. The inset image shows an AFM morphology image of the MoS_2 flake connected to two electrode lines. The scale bar is 5 μm. (c) Raman spectrum of MoS_2. Delta between E_{2g} and A_{1g} is 25 cm^{-1}, which indicates multilayer MoS_2. (d) V_g–I_d transfer characteristics of Au/Ti/MoS_2 FET device, showing *n*-type behavior.

interdigitated Au/Ti electrodes. The height of the flake bridging two electrodes was measured to be approximately 90 nm (Figure 1b). The details of the device fabrication can be found in Figure S1 (SI). The Raman spectrum represents the in-plane vibrational mode (E_{2g}) and the out-of-plane vibrational mode (A_{1g}) from the multilayer MoS_2 film, as shown in Figure 1c.[32] The peak-position difference (Δ) between E_{2g} and A_{1g} was approximately 25 cm^{-1}, which is an indication that the exfoliated MoS_2 flakes are multilayered.[33−35] To determine the electrical properties of the multilayered MoS_2 flakes, we measured the MoS_2 field-effect transistor (FET) characteristics. The V_g–I_d transfer characteristics revealed the *n*-type character of the MoS_2 FET device, which is in good agreement with the results of previous studies (Figure 1d).[11,36] The V_d–I_d characteristics modulated by V_g are also shown in Figure S2 (SI).

The gas-sensing characteristics of the Au/Ti/MoS_2 device based on chemoresistance were explored. Transient resistance responses to NO_2 gas molecules with increasing concentration at various temperatures are shown in Figure 2a. The gas

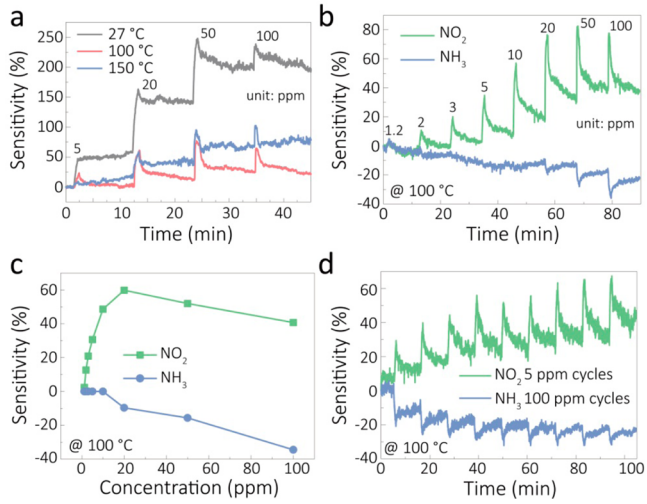

Figure 2. (a) Transient NO_2 gas-sensing characteristics of the Au/Ti/MoS_2 device. The sensitivity and recovery of the device strongly depend on the gas concentrations (5, 20, 50, and 100 ppm) and operating temperatures (27, 100, and 150 °C). (b) Transient responses to NO_2 and NH_3 with 1.2 to 100 ppm. (c) Sensitivity summary of the Au/Ti/MoS_2 device. NO_2 sensitivity is saturated at the relatively low concentration of 20 ppm, whereas NH_3 shows a continual increase in the sensitivity up to 100 ppm. (d) Cycling test for checking the reversible gas-sensing characteristics. The device was tested under two conditions: 5 ppm of NO_2 and 100 ppm of NH_3. Overall, the sensing characteristics were optimized at an operating temperature of 100 °C.

sensitivity is defined as $\Delta R/R_{N2} = (R_g - R_{N2})/R_{N2}$, where R_{N2} and R_g represent the resistance under N_2 gas and the resistance to analyte gas, respectively. When the Au/Ti/MoS_2 sensing device was exposed to NO_2 gas, its resistance began to increase (positive sensitivity). This behavior indicates that the NO_2 molecules attract electrons from the *n*-type MoS_2, leading to an increase in its resistance.[30] Thermal energy is well-known to accelerate the desorption process of gas molecules from a sensing film under inert gas flow.[37,38] With the aid of thermal activation, the recovery rate of the Au/Ti/MoS_2 sensing device was effectively increased. In particular, several sensing-performance parameters, including the sensitivity and recovery, appeared to be optimized at approximately 100 °C; therefore, we chose 100 °C as the operational temperature of the following gas-sensing tests (Figure 2a). As shown in Figure 2b, the transient resistance responses were compared using two analyte gases (NO_2 and NH_3 at concentrations ranging from 1.2 to 100 ppm). In contrast to the resistance change by NO_2 gas molecules, the resistance of the Au/Ti/MoS_2 sensing device decreased with the adsorption of NH_3 gas molecules (negative sensitivity). NH_3 acts as an electron donor, giving an electron to the *n*-type MoS_2, thereby decreasing the resistance of the MoS_2. Overall, the NH_3 sensitivities were observed to be lower than those of NO_2 due to the relatively smaller charge transfer of NH_3.[29,39] Furthermore, the band structures for both valence bands and conduction bands of MoS_2 are not significantly

DOI: 10.1021/acsami.5b04541
ACS Appl. Mater. Interfaces 2015, 7, 16775−16780

altered when NH_3 is adsorbed; however, NO_2-adsorbed MoS_2 induces an unoccupied state above Fermi level.[39] These theoretical results support the reason NO_2 on our MoS_2 gas sensor is much more sensitive than NH_3. Figure 2c is a summary of the strong reliance of the sensitivity on the gas concentration. The surface chemical reaction between the MoS_2 channel and the NO_2 molecules continually increased up to 20 ppm; however, the reaction plateaued for further increases in concentration. In contrast, the sensitivity to NH_3 continually increased to 100 ppm, although the sensitivities below 20 ppm are negligible. This is due to the difference in the adsorption energy and the amount of transferred charge of each molecule to the 2D sensing film.[39] A cycling test via alternating injections of N_2 and the analyte gas is an important requirement for practical sensor applications. In spite of a baseline shift, the gas-sensing characteristics of our Au/Ti/MoS_2 devices were highly stable over many cycling tests upon exposure to 5 ppm of NO_2 and 100 ppm of NH_3 (Figure 2d).

To create flexible sensors, we used a graphene electrode for the devices. Figure 3a shows a schematic drawing of the graphene/MoS_2 device for the gas-sensing test. Exfoliated MoS_2 flakes and patterned graphene lines are used for the channel and the electrodes, respectively (Figure 3b). The morphology

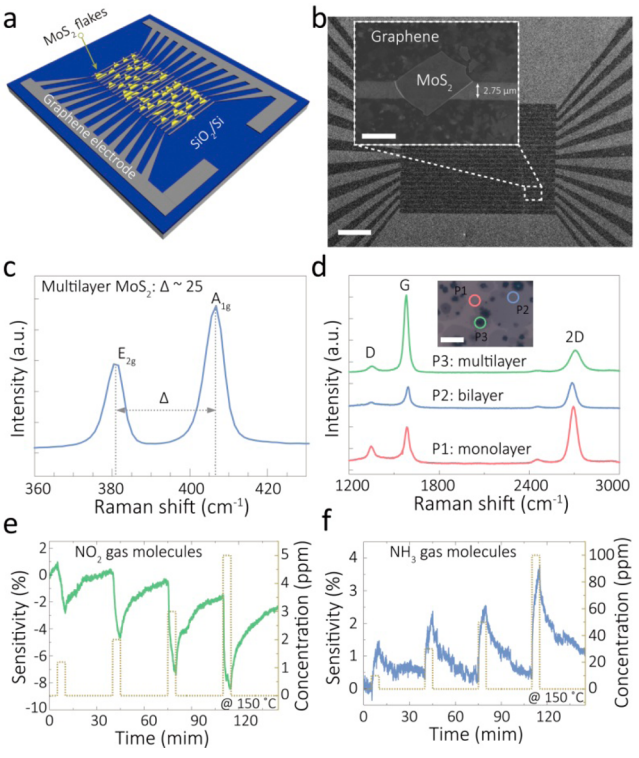

Figure 3. (a) Schematic image of the MoS_2 device with patterned graphene electrodes. (b) SEM image of the MoS_2 device with interdigitated graphene electrodes. The scale bar is 200 μm. The inset image shows the MoS_2 flake bridging two graphene lines. The inset scale bar is 5 μm. (c) Raman spectrum of a MoS_2 flake, indicating its multilayer characteristics. Delta between E_{2g} and A_{1g} is 25 cm^{-1}. (d) Raman spectra of mono-, bi-, and multilayer graphene. The inset shows an optical microscopy image of the graphene marked with P1 (monolayer), P2 (bilayer) and P3 (multilayer) points. The inset scale bar is 20 μm. (e) Transient response to NO_2 gas molecules (1.2 to 5 ppm). (f) Transient response to NH_3 gas molecules (5 to 100 ppm). All gas-sensing tests were performed at an operating temperature of 150 °C.

and thickness of the 2D heterostructure were also analyzed using atomic force microscopy (AFM; Figure S6, SI). To identify the existence of MoS_2 and graphene, Raman spectroscopy was performed. Figure 3c indicates that the exfoliated MoS_2 is multilayered because its peak position difference (Δ) between E_{2g} and A_{1g} was nearly 25 cm^{-1}.[33−35] Figure 3d displays the Raman spectra recorded from various points (P1, P2, and P3 in the inset of Figure 3d) on the graphene film, which can be clearly distinguished in the optical image by contrast differences. The Raman spectrum recorded from CVD-synthesized graphene film has three characteristic bands: D, G, and 2D. The D band is activated in the first-order scattering by in-plane substitutional heteroatoms, vacancies, or other defects.[40] The G and 2D bands are related to the in-plane vibrations of sp^2 carbon atoms in single-layer graphene and the stacking order along the c axis of graphene.[41] Therefore, the graphene thickness can be precisely estimated from the intensity ratio of the 2D band to the G band, I_{2D}/I_G, as follows: $I_{2D}/I_G = 2$ for a monolayer, $I_{2D}/I_G = 1$ for a bilayer, and $I_{2D}/I_G < 1$ for a multilayer structure.[42] Figure 3e displays the sensitivity of the graphene/MoS_2 sensing device under NO_2 gas concentrations of 1.2, 2, 3, and 5 ppm. The gas-sensing performance of the graphene/MoS_2 sensing device, including recovery and sensitivity, was optimized over the operating temperature range of 150 to 200 °C (Figure S3, SI). Thus, the following tests were performed at 150 °C. The difference of the optimized annealing temperature range between two different devices (100 °C for MoS_2 only vs 150 °C for graphene/MoS_2) might come from the introduction of graphene. Molecules can be adsorbed strongly to graphene.[43] Furthermore, the defective and edge sites on our CVD-synthesized graphene inhibit the desorption process of gas molecules, which indicates that higher thermal energy is required compared with the MoS_2 only sensing device. The contribution of the graphene to a gas-sensing property will be discussed later. The injection of NO_2 gas molecules induced negative sensitivity (i.e., the resistance decreased). When the NO_2 gas was turned on, the device resistance tended to recover to the initial resistance value. In contrast, NH_3 gas molecules caused an increase in the device resistance, as shown in Figure 3f. As the NH_3 concentration increased from 5 to 100 ppm, the sensitivity moderately increased. The detection limit for NO_2 was much lower than that of NH_3. This difference is due to the higher adsorption energy of NO_2 molecules compared to that of NH_3 molecules.[44,45] The gas-sensing characteristics of the graphene/MoS_2 devices were reproducible even though there was some device-to-device variation in base resistance and gas sensitivity (Figure S4, SI).

Note that, unlike the n-type behavior of Au/Ti/MoS_2, the graphene/MoS_2 heterojunction gas sensor operated as a p-type device. It is hard to explain the exact origin of majority carrier transition mechanism for each different device (Au/Ti/MoS_2 vs graphene/MoS_2). Nevertheless, we can consider a possible reason: compared to the Ti metal (low work function of 4.3 eV), relatively high work function of graphene (4.7 eV) facilitate hole transport toward valence band edge of MoS_2, which might be responsible for p-type gas-sensing characteristics. On one hand, the sensitivity difference in two devices primarily results from largely different carrier concentration. Apparently, carrier concentration flowing throughout the graphene/MoS_2 device is much higher than that of Au/Ti/MoS_2, which might cause the large difference in gas-sensing characteristics (Table S1, SI). Chemoresistive gas-sensing

DOI: 10.1021/acsami.5b04541
ACS Appl. Mater. Interfaces 2015, 7, 16775−16780

devices rely on a resistance change upon gas injection. The total resistance of the device can be expressed as follows:

$$R_{total} = R_{channel} + R_{contact} + R_{electrode} \quad (1)$$

We can assume that $R_{channel}$ corresponded to the resistance of MoS_2. The two remaining terms ($R_{contact}$ and $R_{electrode}$) then dominate the difference in the gas-sensing behavior. The former ($R_{contact}$) is strongly related to the electronic barrier height (occasionally known as the Schottky barrier height) formed on the active material/electrode interface. The graphene junction to the MoS_2 film usually causes the barrier height to be even lower,[46] which results in less modulation upon gas adsorption than for a metal-MoS_2 junction. The latter ($R_{electrode}$) is usually negligible for metal contacts. However, the resistivity value of a graphene electrode is 2−3 orders of magnitude higher than that of a metal;[47] therefore, the $R_{electrode}$ value cannot be completely excluded in R_{total}. Graphene itself has been reported to sensitively respond to gas molecules. It is concluded that the $R_{electrode}$ value can be changed by gas adsorption, which therefore contributes to the change in R_{total}.

To investigate the potential capacity of a flexible sensor, we fabricated a graphene/MoS_2 gas-sensing device on a polyimide substrate. Figure 4a is an optical image of a bent graphene/MoS_2 gas-sensing device fabricated on a polyimide substrate. The fabrication details are shown in the Experimental Methods section. The inset in Figure 4a shows a semitransparent sensing device before mechanical deformation. As shown in Figure S7 (SI), the device resistance remained stable during a bending test (monitoring the resistance change as a function of the bending cycles or bending radius). The gas response characteristic of the flexible graphene/MoS_2 device at 150 °C was well maintained, without any significant degradation even after 5000 bending cycles. Because the polyimide is highly resistant to thermal stress, this elevated testing temperature could be applied to the flexible device. Furthermore, the flexible graphene/MoS_2 gas sensor device still worked well even after 19 months, showing extraordinary long-term stability (Figure S8, SI). Thus, highly sensitive and reliable performance was demonstrated for these flexible, 2D-heterostructured gas-sensing devices, enabling a promising sensing platform for futuristic wearable electronics.

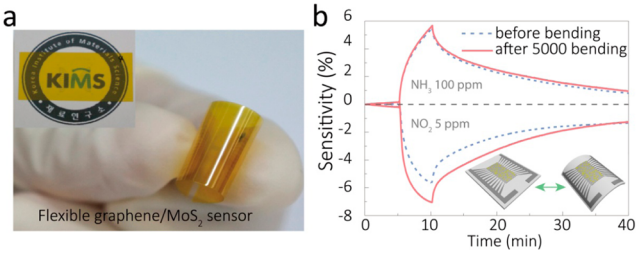

Figure 4. (a) Optical image of a graphene/MoS_2 heterostructured device on a bent polyimide substrate and (inset) the semitransparent sensing device placed on a paper with the KIMS logo. (b) Comparison of the gas response characteristics of the flexible heterostructured device before/after the bending cycle test; (inset) 3D schematic images showing the bending test condition. No serious performance degradation was observed, even after performing 5000 bending cycle tests. The gas-sensing tests were performed at 150 °C. According to the material specification of the PI substrate film used, the temperature range from −269 to 400 °C is acceptable for its applications, which indicates that our annealing condition does not degrade the PI flexible film seriously.

CONCLUSION

We have demonstrated atomically thin, heterostructured gas sensors comprising a combination of exfoliated MoS_2 and CVD graphene. First, we showed that a MoS_2 device with Au/Ti metal electrodes could sensitively detect NO_2 gas molecules above a concentration of 1.2 ppm with excellent gas-sensing stability. Second, we used patterned graphene film instead of a metal for charge collection in a 2D MoS_2-based sensing device. Based on an equation containing several resistance terms, the sensing mechanism of the graphene/MoS_2 device was carefully described. Furthermore, the gas response characteristic of the 2D heterostructure fabricated on a flexible substrate did not exhibit serious degradation, even after 5000 bending cycle tests. This novel 2D heterostructured architecture represents an advance in the development of an important sensing component of futuristic wearable electronics.

EXPERIMENTAL METHODS

CVD Synthesis of Graphene. A Ni/Ti film (300/30 nm) was deposited onto a SiO_2 (300 nm)/Si wafer using an e-beam evaporator. The wafer was placed at the center of a quartz tube and then annealed at 300 °C under a pressure of 800 Torr for 30 min with Ar (2000 sccm)/H_2 (80 sccm) to remove the oxide layer formed on the Ni film. When the temperature reached 900 °C, the graphene film was synthesized onto the Ni film under Ar (2000 sccm)/H_2(80 sccm)/CH_4 (20 sccm) for 5 min, and then the quartz tube was cooled.

Fabrication of Au/Ti/MoS_2 Gas-Sensing Devices. Figure S1 (SI) shows schematic diagrams of the fabrication process on a hard substrate. First, a Si substrate with a thermally grown SiO_2 (100 nm) layer was cleaned using sonication in acetone, isopropyl alcohol (IPA), and DI water for 5 min each. Next, multilayer MoS_2 flakes were transferred to the substrate via mechanical exfoliation. Using conventional photolithography, interdigitated electrode regions with 3 μm channel lengths were patterned. Finally, the metal electrode (Au/Ti = 50/50 nm) was deposited using an e-beam evaporator and then lifted off by acetone.

Fabrication of Graphene/MoS_2 Gas-Sensing Devices. Figure S5 (SI) illustrates the sequential fabrication process of graphene/MoS_2 device. First of all, a Si substrate with a SiO_2 (100 nm) layer was prepared and cleaned. Next, multilayer MoS_2 flakes were mechanically exfoliated onto the substrate. A multilayer graphene film was synthesized on a Si substrate with a Ni film (300 nm) using CVD and was subsequently patterned using conventional photolithography and reactive ion etching (RIE; O_2, 20 sccm; pressure, 200 mTorr; and power, 50 W). The graphene film was then transferred on MoS_2 flakes. After spin-coating a poly(methyl methacrylate) (PMMA, MicroChem, 495k, A2) supporting layer onto the substrate, the device was transferred onto a polyimide substrate by etching the SiO_2 sacrificial layer using buffered oxide etchant. Finally, the PMMA layer was removed by acetone.

ASSOCIATED CONTENT

Supporting Information

Fabrication process of Au/Ti/MoS_2 device, V_d−I_d output characteristics of Au/Ti/MoS_2 FET device, operating temperature dependence of transient gas response characteristics in a graphene/MoS_2 gas-sensing device, device-to-device variation of transient resistance response characteristics, comparison of sensing properties on each different device structure (Au/Ti/MoS_2 vs graphene/MoS_2), fabrication process of a graphene/MoS_2 gas-sensing device, AFM measurement of graphene/MoS_2 contact, bending performance of a graphene/MoS_2 device, and long-term stability of a flexible graphene/MoS_2 device. The Supporting Information is available free of charge

DOI: 10.1021/acsami.5b04541
ACS Appl. Mater. Interfaces 2015, 7, 16775−16780

on the ACS Publications website at DOI: 10.1021/acsami.5b04541.

AUTHOR INFORMATION

Corresponding Authors

*E-mail: bjcho@kims.re.kr.
*E-mail: heungcho@gist.ac.kr.
*E-mail: mghahm@kims.re.kr.

Author Contributions

[‖]These authors contributed equally to this work. B.C., M.G.H., and H.C.K. designed and supervised the experiments. B.C., J.Y., S.K.L., and A.R.K. did the experiments. B.C., J.Y., D.-H.K., S.-G.P., J.-D.K., Y.-J.L., K.-H.L., and B.H.L. analyzed the data. B.C., J.Y., H.C.K., M.G.H., and D.-H.K. co-wrote the paper.

Notes

The authors declare no competing financial interest.

ACKNOWLEDGMENTS

This study was financially supported by the Fundamental Research Program (PNK4210) of the Korean Institute of Materials Science (KIMS). M.G.H. and B.C. are grateful for support from the Basic Science Research Program of the National Research Foundation of Korea (NRF) funded by the Ministry of Science, ICT & Future Planning (NRF-2014R1A1A1006214 and NRF-2014R1A1A1036139).

REFERENCES

(1) Zhang, X.; Qiao, X.-F.; Shi, W.; Wu, J.-B.; Jiang, D.-S.; Tan, P.-H. Phonon and Raman Scattering of Two-Dimensional Transition Metal Dichalcogenides from Monolayer, Multilayer to Bulk Material. *Chem. Soc. Rev.* **2015**, *44*, 2757−2785.

(2) Wang, H.; Yuan, H.; Sae Hong, S.; Li, Y.; Cui, Y. Physical and Chemical Tuning of Two-Dimensional Transition Metal Dichalcogenides. *Chem. Soc. Rev.* **2015**, *44*, 2664−2680.

(3) Wang, Q. H.; Kalantar-Zadeh, K.; Kis, A.; Coleman, J. N.; Strano, M. S. Electronics and Optoelectronics of Two-Dimensional Transition Metal Dichalcogenides. *Nat. Nanotechnol.* **2012**, *7*, 699−712.

(4) Fiori, G.; Bonaccorso, F.; Iannaccone, G.; Palacios, T.; Neumaier, D.; Seabaugh, A.; Banerjee, S. K.; Colombo, L. Electronics Based on Two-Dimensional Materials. *Nat. Nanotechnol.* **2014**, *9*, 768−779.

(5) Tan, C.; Liu, Z.; Huang, W.; Zhang, H. Non-Volatile Resistive Memory Devices Based on Solution-Processed Ultrathin Two-Dimensional Nanomaterials. *Chem. Soc. Rev.* **2015**, *44*, 2615−2628.

(6) Tan, C.; Zhang, H. Two-Dimensional Transition Metal Dichalcogenide Nanosheet-Based Composites. *Chem. Soc. Rev.* **2015**, *44*, 2713−2731.

(7) Li, H.; Wu, J.; Yin, Z.; Zhang, H. Preparation and Applications of Mechanically Exfoliated Single-Layer and Multilayer MoS_2 and WSe_2 Nanosheets. *Acc. Chem. Res.* **2014**, *47*, 1067−1075.

(8) Huang, X.; Tan, C.; Yin, Z.; Zhang, H. 25th Anniversary Article: Hybrid Nanostructures Based on Two-Dimensional Nanomaterials. *Adv. Mater.* **2014**, *26*, 2185−2204.

(9) Huang, X.; Zeng, Z.; Zhang, H. Metal Dichalcogenide Nanosheets: Preparation, Properties and Applications. *Chem. Soc. Rev.* **2013**, *42*, 1934−1946.

(10) Novoselov, K. S.; Jiang, D.; Schedin, F.; Booth, T. J.; Khotkevich, V. V.; Morozov, S. V.; Geim, a K. Two-Dimensional Atomic Crystals. *Proc. Natl. Acad. Sci. U. S. A.* **2005**, *102*, 10451−10453.

(11) Radisavljevic, B.; Radenovic, A.; Brivio, J.; Giacometti, V.; Kis, A. Single-Layer MoS_2 Transistors. *Nat. Nanotechnol.* **2011**, *6*, 147−150.

(12) Lee, G.; Yu, Y.; Cui, X.; Petrone, N.; Lee, C.; Choi, S.; Lee, D.; Lee, C.; Yoo, W. J.; Watanabe, K.; Taniguchi, T.; Nuckolls, C.; Kim, P.; Hone, J. Flexible and Transparent MoS_2 Field- Effect Transistors on Hexagonal Boron Nitride-Graphene Heterostructures. *ACS Nano* **2013**, *7*, 7931−7936.

(13) Wang, H.; Yu, L.; Lee, Y.-H.; Shi, Y.; Hsu, A.; Chin, M. L.; Li, L.-J.; Dubey, M.; Kong, J.; Palacios, T. Integrated Circuits Based on Bilayer MoS_2 Transistors. *Nano Lett.* **2012**, *12*, 4674−4680.

(14) Wu, J.; Li, H.; Yin, Z.; Li, H.; Liu, J.; Cao, X.; Zhang, Q.; Zhang, H. Layer Thinning and Etching of Mechanically Exfoliated MoS_2 Nanosheets by Thermal Annealing in Air. *Small* **2013**, *9*, 3314−3319.

(15) Li, H.; Lu, G.; Yin, Z.; He, Q.; Li, H.; Zhang, Q.; Zhang, H. Optical Identification of Single- and Few-Layer MoS_2 Sheets. *Small* **2012**, *8*, 682−686.

(16) Lopez-Sanchez, O.; Lembke, D.; Kayci, M.; Radenovic, A.; Kis, A. Ultrasensitive Photodetectors Based on Monolayer MoS_2. *Nat. Nanotechnol.* **2013**, *8*, 497−501.

(17) Yin, Z.; Li, H.; Li, H.; Jiang, L.; Shi, Y.; Sun, Y.; Lu, G.; Zhang, Q.; Chen, X.; Zhang, H. Single-Layer MoS_2 Phototransistors. *ACS Nano* **2012**, *6*, 74−80.

(18) Late, D. J.; Huang, Y.; Liu, B.; Acharya, J.; Shirodkar, S. N.; Luo, J. Sensing Behavior of Atomically Thin-Layered MoS_2 Transistors. *ACS Nano* **2013**, *7*, 4879−4891.

(19) Perkins, F. K.; Friedman, a L.; Cobas, E.; Campbell, P. M.; Jernigan, G. G.; Jonker, B. T. Chemical Vapor Sensing with Monolayer MoS_2. *Nano Lett.* **2013**, *13*, 668−673.

(20) Li, H.; Yin, Z.; He, Q.; Li, H.; Huang, X.; Lu, G.; Fam, D. W. H.; Tok, A. I. Y.; Zhang, Q.; Zhang, H. Fabrication of Single- and Multilayer MoS_2 Film-Based Field-Effect Transistors for Sensing NO at Room Temperature. *Small* **2012**, *8*, 63−67.

(21) He, Q.; Zeng, Z.; Yin, Z.; Li, H.; Wu, S.; Huang, X.; Zhang, H. Fabrication of Flexible MoS_2 Thin-Film Transistor Arrays for Practical Gas-Sensing Applications. *Small* **2012**, *8*, 2994−2999.

(22) Geim, a K.; Grigorieva, I. V. Van Der Waals Heterostructures. *Nature* **2013**, *499*, 419−425.

(23) Lee, C.-H.; Lee, G.-H.; van der Zande, A. M.; Chen, W.; Li, Y.; Han, M.; Cui, X.; Arefe, G.; Nuckolls, C.; Heinz, T. F.; Guo, J.; Hone, J.; Kim, P. Atomically Thin P−n Junctions with van Der Waals Heterointerfaces. *Nat. Nanotechnol.* **2014**, *9*, 676−681.

(24) Hong, X.; Kim, J.; Shi, S.-F.; Zhang, Y.; Jin, C.; Sun, Y.; Tongay, S.; Wu, J.; Zhang, Y.; Wang, F. Ultrafast Charge Transfer in Atomically Thin MoS_2/WS_2 Heterostructures. *Nat. Nanotechnol.* **2014**, *9*, 682−686.

(25) Duesberg, G. S. Heterojunctions in 2D Semiconductors: A Perfect Match. *Nat. Mater.* **2014**, *13*, 1075−1076.

(26) Roy, T.; Tosun, M.; Cao, X.; Fang, H.; Lien, D.; Zhao, P.; Al, R. O. Y. E. T. Dual-Gated MoS_2 /WSe_2 van Der Waals Tunnel Diodes and Transistors. *ACS Nano* **2015**, *9*, 2071−2079.

(27) Britnell, L.; Gorbachev, R. V.; Jalil, R.; Belle, B. D.; Schedin, F.; Mishchenko, A.; Georgiou, T.; Katsnelson, M. I.; Eaves, L.; Morozov, S. V.; Peres, N. M. R.; Leist, J.; Geim, a K.; Novoselov, K. S.; Ponomarenko, L. A. Field-Effect Tunneling Transistor Based on Vertical Graphene Heterostructures. *Science* **2012**, *335*, 947−950.

(28) Yu, W. J.; Li, Z.; Zhou, H.; Chen, Y.; Wang, Y.; Huang, Y.; Duan, X. Vertically Stacked Multi-Heterostructures of Layered Materials for Logic Transistors and Complementary Inverters. *Nat. Mater.* **2013**, *12*, 246−252.

(29) Cho, B.; Kim, A. R.; Park, Y.; Yoon, J.; Lee, Y.-J.; Lee, S.; Yoo, T. J.; Kang, C. G.; Lee, B. H.; Ko, H. C.; Kim, D.-H.; Hahm, M. G. Bifunctional Sensing Characteristics of Chemical Vapor Deposition Synthesized Atomic-Layered MoS_2. *ACS Appl. Mater. Interfaces* **2015**, *7*, 2952−2959.

(30) Cho, B.; Hahm, M. G.; Choi, M.; Yoon, J.; Kim, A. R.; Lee, Y.-J.; Park, S.-G.; Kwon, J.-D.; Kim, C. S.; Song, M.; Jeong, Y.; Nam, K.-S.; Lee, S.; Yoo, T. J.; Kang, C. G.; Lee, B. H.; Ko, H. C.; Ajayan, P. M.; Kim, D.-H. Charge-Transfer-Based Gas Sensing Using Atomic-Layer MoS_2. *Sci. Rep.* **2015**, *5*, 8052.

(31) Schedin, F.; Geim, A. K.; Morozov, S. V.; Hill, E. W.; Blake, P.; Katsnelson, M. I.; Novoselov, K. S. Detection of Individual Gas Molecules Adsorbed on Graphene. *Nat. Mater.* **2007**, *6*, 652−655.

(32) Bertrand, P. A. Surface-Phonon Dispersion of MoS_2. *Phys. Rev. B: Condens. Matter Mater. Phys.* **1991**, *44*, 5745−5749.

(33) Liu, K.-K.; Zhang, W.; Lee, Y.-H.; Lin, Y.-C.; Chang, M.-T.; Su, C.-Y.; Chang, C.-S.; Li, H.; Shi, Y.; Zhang, H.; Lai, C.-S.; Li, L.-J.

DOI: 10.1021/acsami.5b04541
ACS Appl. Mater. Interfaces 2015, 7, 16775−16780

Growth of Large-Area and Highly Crystalline MoS_2 Thin Layers on Insulating Substrates. *Nano Lett.* **2012**, *12*, 1538−1544.
(34) Li, S.; Miyazaki, H.; Song, H.; Kuramochi, H.; Nakaharai, S.; Tsukagoshi, K. Quantitative Raman Spectrum and Reliable Thickness Identification for Atomic Layers on Insulating Substrates. *ACS Nano* **2012**, *6*, 7381−7388.
(35) Liu, Y.; Nan, H.; Wu, X.; Pan, W.; Wang, W.; Bai, J.; Zhao, W.; Sun, L.; Wang, X.; Ni, Z. Layer-by-Layer Thinning of MoS_2 by Plasma. *ACS Nano* **2013**, *7*, 4202−4209.
(36) Dolui, K.; Rungger, I.; Sanvito, S. Origin of the N-Type and P-Type Conductivity of MoS_2 Monolayers on a SiO_2 Substrate. *Phys. Rev. B: Condens. Matter Mater. Phys.* **2013**, *87*, 165402.
(37) Yavari, F.; Chen, Z.; Thomas, A. V.; Ren, W.; Cheng, H.-M.; Koratkar, N. High Sensitivity Gas Detection Using a Macroscopic Three-Dimensional Graphene Foam Network. *Sci. Rep.* **2011**, *1*, 166.
(38) Choi, H.; Choi, J. S.; Kim, J.-S.; Choe, J.-H.; Chung, K. H.; Shin, J.-W.; Kim, J. T.; Youn, D.-H.; Kim, K.-C.; Lee, J.-I.; Choi, S.-Y.; Kim, P.; Choi, C.-G.; Yu, Y.-J. Flexible and Transparent Gas Molecule Sensor Integrated with Sensing and Heating Graphene Layers. *Small* **2014**, *10*, 3685−3691.
(39) Yue, Q.; Shao, Z.; Chang, S.; Li, J. Adsorption of Gas Molecules on Monolayer MoS_2 and Effect of Applied Electric Field. *Nanoscale Res. Lett.* **2013**, *8*, 425.
(40) Thomsen, C.; Reich, S. Double Resonant Raman Scattering in Graphite. *Phys. Rev. Lett.* **2000**, *85*, 5214−5217.
(41) Cançado, L.; Reina, A.; Kong, J.; Dresselhaus, M. Geometrical Approach for the Study of G′ Band in the Raman Spectrum of Monolayer Graphene, Bilayer Graphene, and Bulk Graphite. *Phys. Rev. B: Condens. Matter Mater. Phys.* **2008**, *77*, 245408.
(42) Li, X.; Cai, W.; An, J.; Kim, S.; Nah, J.; Yang, D.; Piner, R.; Velamakanni, A.; Jung, I.; Tutuc, E.; Banerjee, S. K.; Colombo, L.; Ruoff, R. S. Large-Area Synthesis of High-Quality and Uniform Graphene Films on Copper Foils. *Science* **2009**, *324*, 1312−1314.
(43) Randeniya, L. K.; Shi, H.; Barnard, A. S.; Fang, J.; Martin, P. J.; Ostrikov, K. K. Harnessing the Influence of Reactive Edges and Defects of Graphene Substrates for Achieving Complete Cycle of Room-Temperature Molecular Sensing. *Small* **2013**, *9*, 3993−3999.
(44) Zhang, Y.-H.; Chen, Y.-B.; Zhou, K.-G.; Liu, C.-H.; Zeng, J.; Zhang, H.-L.; Peng, Y. Improving Gas Sensing Properties of Graphene by Introducing Dopants and Defects: A First-Principles Study. *Nanotechnology* **2009**, *20*, 185504.
(45) Zhou, M.; Lu, Y.-H.; Cai, Y.-Q.; Zhang, C.; Feng, Y.-P. Adsorption of Gas Molecules on Transition Metal Embedded Graphene: A Search for High-Performance Graphene-Based Catalysts and Gas Sensors. *Nanotechnology* **2011**, *22*, 385502.
(46) Kwak, J. Y.; Hwang, J.; Calderon, B.; Alsalman, H.; Munoz, N.; Schutter, B.; Spencer, M. G. Electrical Characteristics of Multilayer MoS_2 FET's with MoS_2/Graphene Heterojunction Contacts. *Nano Lett.* **2014**, *14*, 4511−4516.
(47) Cho, B.; Yoon, J.; Hahm, M. G.; Kim, D.-H.; Kim, A. R.; Kahng, Y. H.; Park, S.-W.; Lee, Y.-J.; Park, S.-G.; Kwon, J.-D.; Kim, C. S.; Song, M.; Jeong, Y.; Nam, K.-S.; Ko, H. C. Graphene-Based Gas Sensor: Metal Decoration Effect and Application to a Flexible Device. *J. Mater. Chem. C* **2014**, *2*, 5280−5285.

DOI: 10.1021/acsami.5b04541
ACS Appl. Mater. Interfaces 2015, 7, 16775−16780